

NINTH EUROPEAN ROTORCRAFT FORUM

Paper No. B

A HOLOGRAPHIC INTERFEROMETRY TECHNIQUE FOR MEASURING
TRANSONIC FLOW NEAR A ROTOR BLADE

JOHN K. KITTLESON

Aeromechanics Laboratory
U.S. Army Aviation R&D Command
NASA Ames Research Center
Moffett Field, California 94035, U.S.A.

September 13-15, 1983

STRESA, ITALY

A HOLOGRAPHIC INTERFEROMETRY TECHNIQUE FOR MEASURING
TRANSONIC FLOW NEAR A ROTOR BLADE

John K. Kittleson
Aeromechanics Laboratory
U.S. Army Aviation R&D Command
NASA Ames Research Center
Moffett Field, California 94035, U.S.A.

ABSTRACT

A technique that uses holographic interferometry to record the first interferograms of the flow near a hovering transonic rotor blade is presented. A pulsed ruby laser is used to record interferograms of a 2-ft-diam field of view near a rotor tip operating at a tip Mach number of 0.90. Several interferograms, recorded along planes perpendicular to the rotor's tip-path-plane at various azimuthal angles around the flow, are presented. These interferograms yield quantitative information about shock structure and location, flow separation, and radiated noise that will help helicopter researchers understand the complexities of the flow around high-speed rotor blades and thus improve performance and reduce noise.

1. INTRODUCTION

On many modern helicopters, the speed of the advancing blade tip enters the transonic range during forward flight. At these high Mach numbers, the rotor blade is subjected to compressibility effects caused by shock waves developing near the tip region. Much theoretical work has been done recently in efforts to understand the causes of these effects; however, because of the complexity of the problem and lack of detailed experimental information of the flow itself, accurate design tools for transonic rotor-blade designs are not yet available.

It is well known that the presence of the shock wave rapidly increases the aerodynamic drag (Fig. 1). Energy is dissipated in the shock wave, giving rise to wave drag. The shock also causes an unfavorable

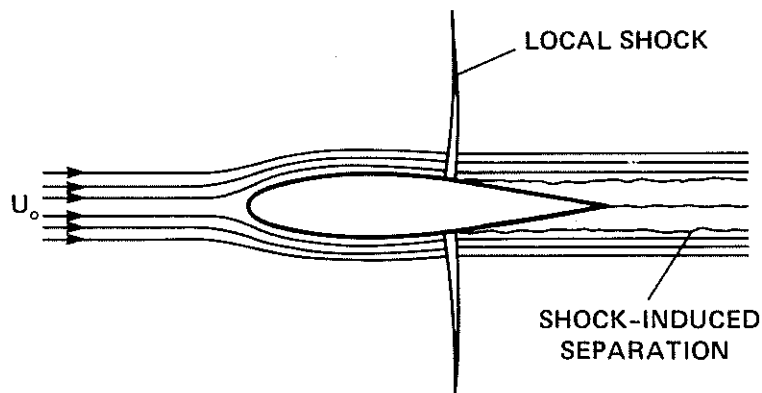


Fig. 1. A sketch of the aerodynamic environment of a transonic rotor.

pressure gradient to develop which can separate the flow at the foot of the shock. This separated flow causes increased drag and its attendant problems. Another effect of local shocks is sudden "large changes" in pitching moment that can excite the blade torsional frequency. As the blade rotates in forward flight, its tip Mach number and angle of attack are varying. The shocks appear on the advancing side of the rotor disc and can make large chordwise movements, sometimes moving in opposite directions on the upper and lower surfaces as the Mach number and angle of attack change during a revolution. The changing shock positions on the upper and lower surfaces cause an unsteady loading, which produces fluctuating pitching moments. These can cause unexpected blade motions, oscillating loads on the pitch links, and vibrations throughout the entire aircraft. In addition, the shock wave on an advancing blade surface can "delocalize" and extend directly to the acoustic far-field.¹ Large amounts of acoustic energy radiate in front of the helicopter near the tip-path-plane. This is called impulsive noise, the most annoying and easily detectable sound generated by a helicopter.

Theoretical approaches to describing the transonic rotor flow field have looked very promising.² Numerical codes have been developed³ which compare favorably with blade pressure measurements. However, the numerical work to date has not been verified off the surface of the blade, hindering further quantification of the theory. Unfortunately, pressure-instrumented airfoils are expensive and difficult to fabricate — especially in scale models. In addition, large centrifugal loads and blade stress make accurate measurements difficult.

Other previous attempts to measure the flow field have also been severely limited. Hot-wire anemometry requires that a probe be placed in the field, therefore disturbing the flow. Laser velocimetry requires seeding of the flow. If the seeds cannot follow the flow faithfully (i.e., when shock waves are present), accurate measurements are difficult to make. Because both of the above methods can only be used to make point-by-point measurements, they require large amounts of running time to survey the three-dimensional flow field of a rotor. This is a distinct disadvantage for rotor testing. Schlieren and shadowgraph photography provide only a qualitative two-dimensional representation of a three-dimensional flow. Mach-Zehnder interferometry provides quantitative information, but is extremely difficult to use in a large-scale experiment. Clearly, another experimental technique which overcomes these limitations must be employed.

This paper presents a method of using holographic interferometry with computerized tomography to measure the flow near a transonic rotor blade. Holographic interferometry is a very effective diagnostic technique in transonic flows.⁴ Previous investigations^{5,6} of two-dimensional flows over airfoils have shown that good quantitative information can be obtained. However, the transonic flow around a helicopter rotor blade is three dimensional and requires the use of tomography to extract the correct information from the interferograms. To date, most applications of this technique have been limited to axisymmetric flow or to a simple three-dimensional flow with a small model under ideal laboratory conditions.^{7,8} This is the first time the method has been applied to measuring the flow near a hovering rotor. The experiment proved to be very challenging since the flow under study was transonic, large scale, and three dimensional.

In this paper, quantitative holographic interferograms near a transonic hovering rotor tip are presented. First, a brief introduction to the principles of holography, holographic interferometry, and

tomography is provided to highlight the advantages of using this technique. Next, the experimental equipment and the procedure of recording the holographic interferograms are described. And finally, interferograms are presented with a qualitative explanation of their meaning and a brief discussion of how they can be analyzed to yield quantitative information.

2. BACKGROUND CONCEPTS

The success of this experiment is dependent upon recording high-quality interferograms from multiple viewing angles of the desired flow; the interferograms serve as data for a tomography code. To understand why this technique can be used to measure the transonic flow around a rotor blade, it is helpful to be familiar with some basic optical principles.

Holography is a two-step imaging process in which diffracted light waves are recorded and reconstructed.^{9,10} The first step is to record, or store the hologram. This is accomplished by dividing a single coherent laser beam into two beams and exposing a photographic film to these two light waves, as shown in Fig. 2a. The wave of interest is called the object wave; it passes through the field that is to be measured (the air near the rotor blade in this experiment). The other wave is called the reference wave; it passes around the field of interest. Thus, a high-frequency interference pattern is recorded on the photographic film by adding a coherent reference wave to the object wave. The irradiance at the film plane is

$$\begin{aligned} I &= |U_R + U_O|^2 \\ &= I_R + I_O + U_R^* U_O + U_R U_O^* \end{aligned} \quad (1)$$

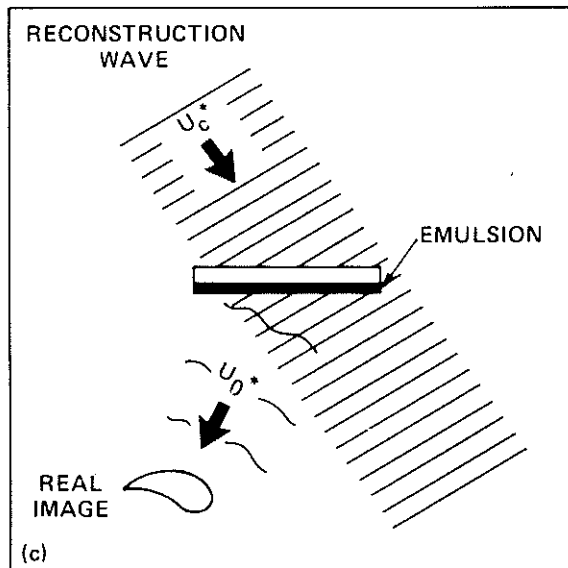
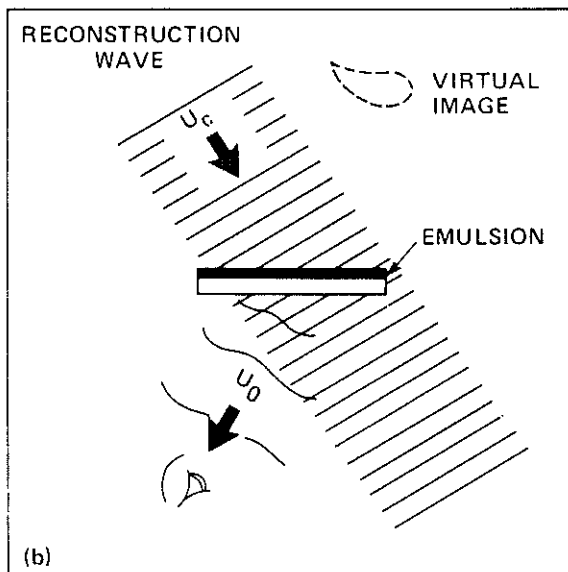
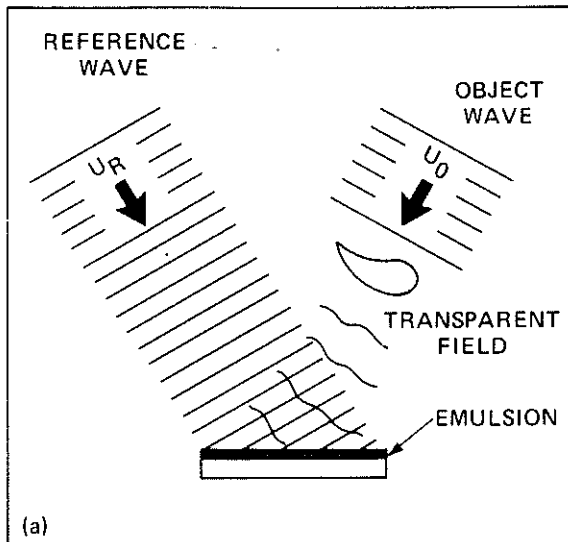
where U_R is the complex amplitude of the reference wave, U_O is the complex amplitude of the object wave, I_R and I_O are amplitude squares of the reference and object waves, and the asterisk indicates a conjugate wave. The last two terms of Eq. (1) represent the interference pattern recorded on the film, which contains both amplitude and phase information of the two waves. The film is then developed, after which it is called a hologram; a hologram may be thought of as a complicated diffraction grating. The amplitude transmittance of the hologram is

$$t = \beta(I_R + I_O) + \beta U_R^* U_O + \beta U_R U_O^*$$

where β is a property of the film.

The second step in holography is to reconstruct, or play back the hologram. This can be accomplished in two ways. In the first, the hologram is illuminated with a reconstruction wave U_C that is identical to the reference wave, as shown in Fig. 2b. In this case, the transmitted light is

$$\begin{aligned} U_I &= U_C t \\ &= \beta U_C (I_R + I_O) + \beta U_R^* U_C U_O + \beta U_R U_C U_O^* \end{aligned} \quad (2)$$



Physically, the first term in Eq. (2) represents the wave that is transmitted directly through the hologram. The second and third terms represent two first-order diffracted waves. The second, and most important, term of Eq. (2) can be written as $(\beta U_R^* U_c) U_o$, which is a replica of the original object wave. Thus, a virtual image of the original object has been reproduced.

In the second method of reconstructing the hologram, the hologram is illuminated with a reconstruction wave U_c^* that is the conjugate of the reference wave, as shown in Fig. 2c. This can often be accomplished by rotating the hologram 180° about the vertical axis. The transmitted light is then given by

$$\begin{aligned}
 U_I &= U_c^* t \\
 &= \beta U_c^* (I_R + I_o) + \beta U_R^* U_c^* U_o \\
 &\quad + \beta U_R U_c U_o^* \quad (3)
 \end{aligned}$$

The last term of Eq. (3) can be written as $(\beta U_R U_c^*) U_o^*$, which represents a diffracted wave that is conjugate to the original object wave. Physically, this wave produces a real image that can be photographed without the use of a lens by placing a sheet of photographic film in the real-image space.

Fig. 2. Optical holography recording and reconstructing. (a) Recording the hologram. (b) Reconstruction of the true, virtual image. (c) Reconstruction of the conjugate, real image.

Several important characteristics of holography are applicable to the experiment at hand. There are very few geometrical constraints in a holographic optical system, thus holography can be applied in a large-scale, nonlaboratory environment. Note also that the recording and reconstruction of the hologram can be done in completely different locations if the reference wave can be reproduced. This allows the reconstruction to be done in a laboratory, far from the harsh environment where the hologram was recorded. It should also be remembered that the reference wave serves only as a method of storing and playing back the object wave. Thus, a hologram does not produce quantitative information about the field of interest. To obtain quantitative information (in the form of interference fringes) an interferogram must be made.

Holographic interferometry is the interferometric comparison of two object waves that are recorded holographically. The two object waves are recorded sequentially in time with double-exposure holographic interferometry. The interferogram is recorded by first exposing a photographic film to a reference wave and an "undisturbed" object wave, as shown in Fig. 3a. Later in time, the same photographic plate is exposed to a reference wave and a second "disturbed" object wave, as shown in Fig. 3b. The irradiance at the film plane is

$$I = |U_R + U_{O1}|^2 + |U_R + U_{O2}|^2$$

$$= 2I_R + I_{O1} + I_{O2} + U_R^*(U_{O1} + U_{O2}) + U_R(U_{O1} + U_{O2})^* \quad (4)$$

where U_{O1} is the complex amplitude of the undisturbed object wave, and U_{O2} is the complex amplitude of the disturbed object wave. As in single-exposure holography, the last two terms of Eq. (4) represent the interference pattern recorded on the film, which contains both amplitude and phase information of the two reference and two object waves. The amplitude transmittance of the developed film, called a holographic interferogram, is

$$t = \beta(2I_R + I_{O1} + I_{O2}) + \beta U_R^*(U_{O1} + U_{O2}) + \beta U_R(U_{O1} + U_{O2})^*$$

When the reconstruction wave U_C illuminates the interferogram as shown in Fig. 3c, the transmitted light is

$$U_I = U_C t$$

$$= \beta U_C(2I_R + I_{O1} + I_{O2}) + \beta U_R^* U_C(U_{O1} + U_{O2}) + \beta U_R U_C(U_{O1} + U_{O2})^* \quad (5)$$

The second term of Eq. (5) is the "composite" virtual image reconstruction of the two object waves ($U_{O1} + U_{O2}$). By illuminating the interferogram with a reconstruction wave U_C^* (Fig. 3d), the transmitted light is

$$U_I = U_C^* t$$

$$= \beta U_C^*(2I_R + I_{O1} + I_{O2}) + \beta U_R^* U_C^*(U_{O1} + U_{O2}) + \beta U_R U_C^*(U_{O1} + U_{O2})^* \quad (6)$$

The third term of Eq. (6) is the composite real-image reconstruction of the two object waves. It is this image that is photographed and presented in this paper. Note that the irradiance of the reconstructed wave is proportional to

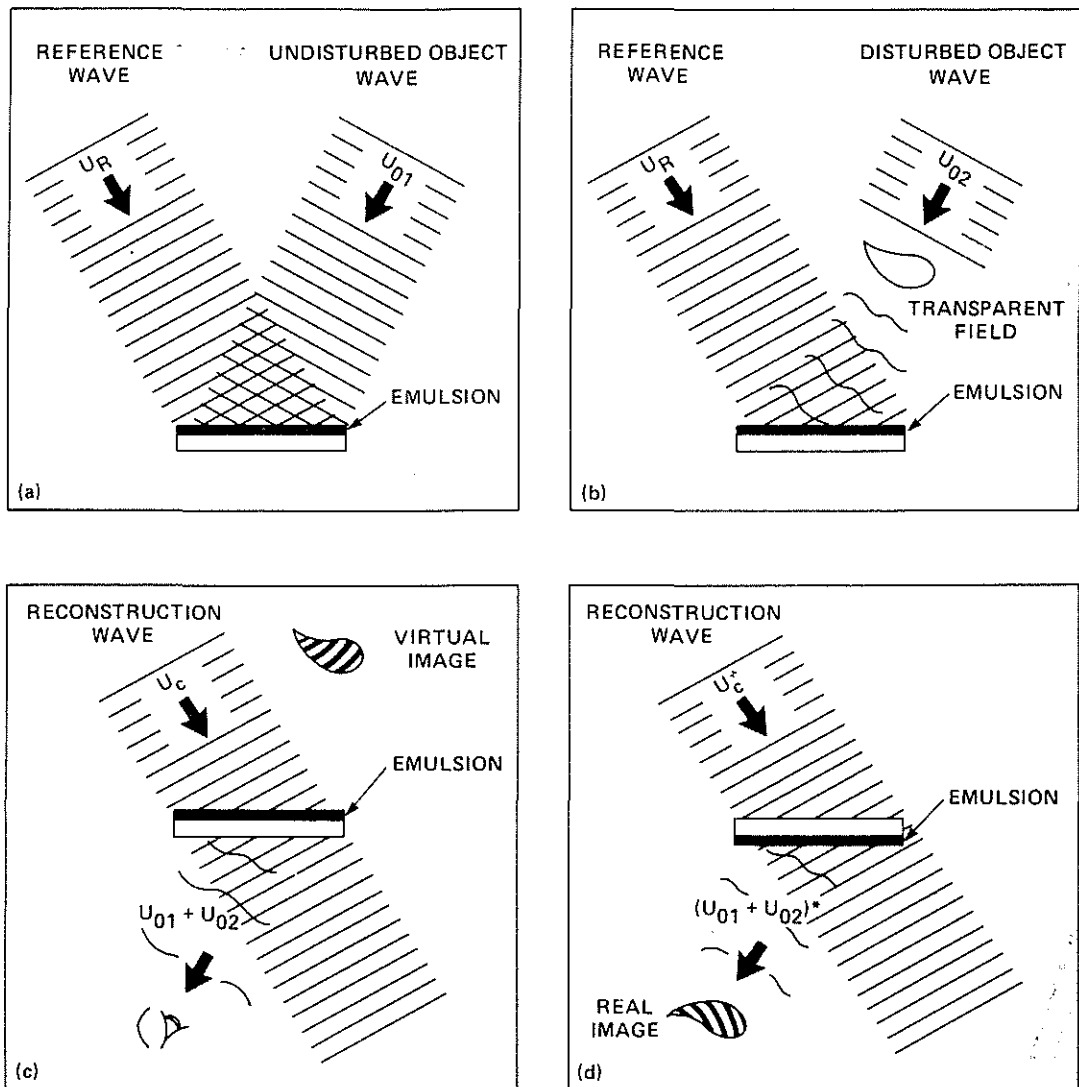


Fig. 3. Double-exposure holographic interferometry. (a) First-exposure recording. (b) Second-exposure recording. (c) Reconstruction of the virtual image. (d) Reconstruction of the real image.

$$I = |U_{01} + U_{02}|^2$$

which can be written as^{9,10}

$$I = 2A^2[1 + \cos(\Delta\phi)] \quad (7)$$

where A is the amplitude of the two object waves, and $\Delta\phi$ is the optical path-length difference between the two object waves. Equation (7) represents an interferogram with a fringe pattern of dark and bright fringes of constant values of $\Delta\phi$, where $\Delta\phi$ is given by

$$\Delta\phi = \int_s [n(x,y,z) - n_0] ds = N\lambda \quad (8)$$

where $n(x,y,z)$ and n_0 are the index of refraction of the disturbed and undisturbed field (air in this experiment), N is the fringe order number, and λ is the wavelength of the ruby laser ($0.6943 \mu\text{m}$). To determine the properties of the flow field of interest, Eq. (8) must be inverted and solved for $n(x,y,z)$, the index of refraction at any desired point in the field.

The main reason for using holographic interferometry is that it possesses a property called cancellation of path-length errors. The simple example of Fig. 4 (from Ref. 9) illustrates this property by demonstrating the difference between a Mach-Zehnder and a holographic interferometer. This figure shows two interferograms of a thermal plume above a heated wire (the wire being perpendicular to the page). Figure 4a is an interferogram made with a Mach-Zehnder interferometer using low-quality optics. In this case the interfering light waves are divided spatially. That is, the two interfering waves are recorded simultaneously but travel different paths in the optical system, as shown in Fig. 5a. Any differences in the path lengths in the optical system would give rise to extraneous fringes (leaving a useless interferogram), which could be eliminated only by using very high-quality optics. This is a very difficult and expensive requirement to meet when using large optical components such as are used in this experiment. However, in a holographic interferometer, the interfering waves are divided temporally. That is, the two interfering (object) waves are recorded at two different times but travel the same path through the optical system, as shown in Fig. 5b. (Recall that the reference wave serves only to store and play back the interferogram.) Since there is no difference in the path lengths of the two interfering object waves in the optical system, only changes in the path lengths caused by the different states of the test field are displayed as fringes in the interferogram. This leaves a useful interferogram (Fig. 4b), even though low-quality optics are used. Therefore, holographic interferometry can be employed in a large-scale experiment using relatively low-quality optics and still yield high-quality interferograms of the field of interest.

As an optical ray passes through a transparent field, its optical path length is changed. In a double-exposure holographic interferogram, the optical path-length difference ($\Delta\phi$) between the two flow states is recorded on photographic film at point P in Fig. 6, and is given by

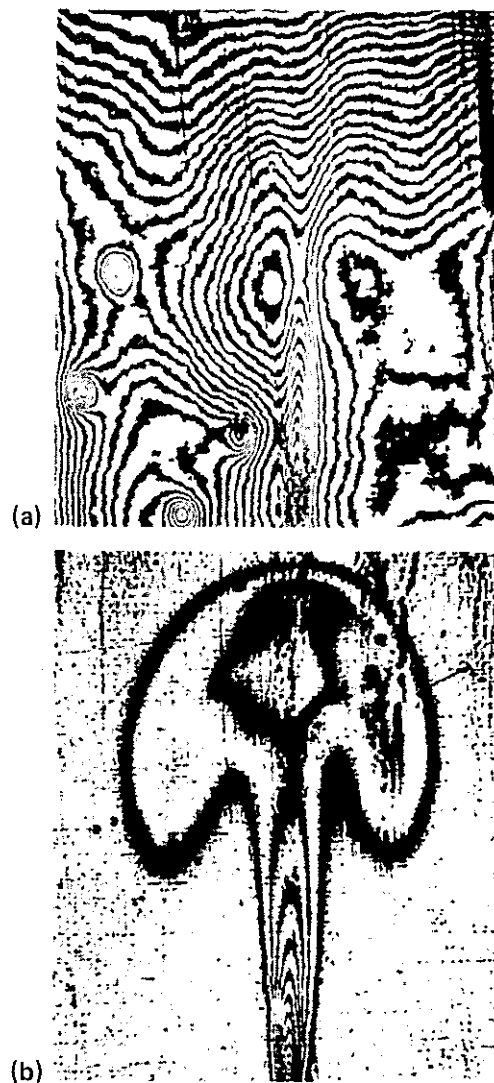


Fig. 4. Effect of low-quality optics. (a) Interferogram formed with a Mach-Zehnder interferometer. (b) Interferogram formed with a holographic interferometer.

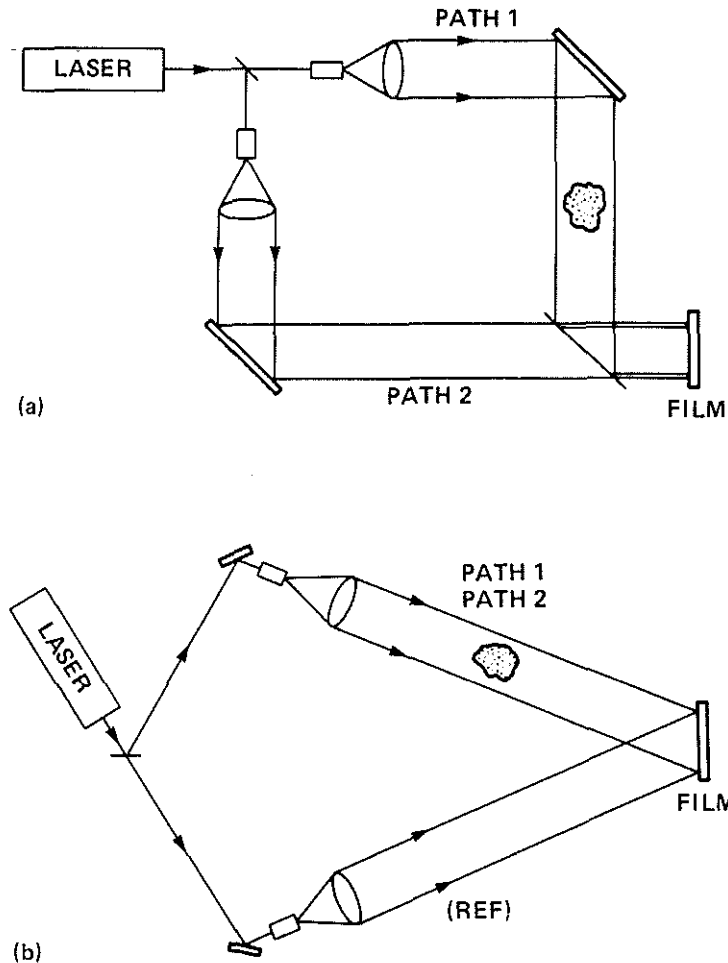


Fig. 5. Path differences of interfering waves. (a) Waves travel different paths at the same time in a Mach-Zehnder interferometer. (b) Waves travel the same path at two different times in a holographic interferometer. (Lower beam is reference wave.)

Eq. (8). Note that $\Delta\phi$ is an integrated value along the optical ray. In a two-dimensional flow (i.e., the example of Fig. 4 or the flow over a fixed airfoil in a wind tunnel), the evaluation of this integral is straightforward. Since the index of refraction is constant across the width of the test section L , Eq. (8) becomes

$$n(x,y) = n_0 + \frac{N\lambda}{L} \quad (9)$$

Thus, in a two-dimensional flow, the fringes on an interferogram are contours of constant index of refraction and the index of refraction at any point in the flow field can be obtained from a single interferogram.

However, since the transonic flow near a rotor blade is three dimensional, Eq. (9) cannot be used. To invert Eq. (8) and solve for the index of refraction at a specific point in the flow, tomography must be used. Tomography is a technique for reconstructing a three-dimensional field from its two-dimensional projections. A projection is what is recorded on an interferogram. One tomography method uses convolution to back-project

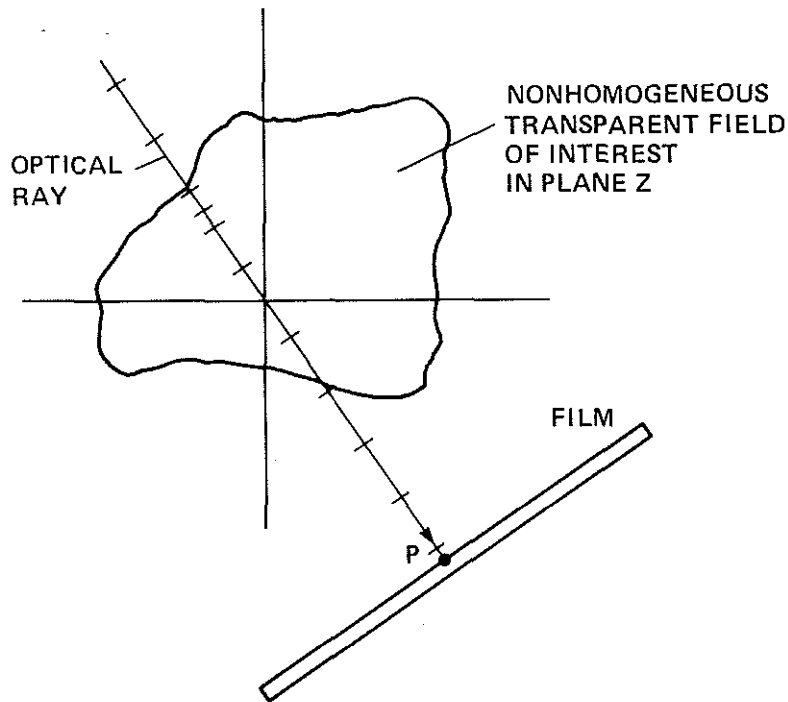


Fig. 6. Detection of an integrated phase change in a transparent field.

and filter a projection onto the three-dimensional space. Another tomography method discretizes the line integral of Eq. (8) and solves a set of linear algebraic equations to reconstruct the three-dimensional field. The subject of tomography is a topic in itself and will not be discussed in detail in this paper. However, all tomography codes require multidirectional data of the field of interest. Therefore, to obtain quantitative information at a desired point in the transonic flow near a rotor blade, several interferograms at various angles around the flow (Fig. 7) must be recorded to serve as data to a tomography code.

3. EXPERIMENTAL METHOD

A schematic drawing of the basic optical system required to record holographic interferograms near a scaled rotor blade in the Aeromechanics Laboratory Anechoic Hover Chamber is shown in Fig. 8. A ruby laser with a pulse width of 20 nsec is used to "freeze" the rotating blade at any desired azimuthal angle. The laser beam is divided into two parts with a beam splitter at the outlet of the laser. The object beam is expanded with a microscope objective lens to fill a 24-in.-diam spherical mirror. Since the foci of the objective lens and spherical mirror coincide, a collimated plane wave is formed as the beam passes through the rotor area. The beam then strikes a second 24-in.-diam spherical mirror, emerges as a converging wave, and illuminates a 4- by 5-in. photographic plate. The reference beam is lengthened by striking several plane mirrors. This beam must be lengthened such that the difference in the path lengths of the object and reference beams be less than the coherence length of the laser (one of the very few, and easily met, geometrical constraints in a holographic system). The reference beam is then expanded by an objective lens, collimated with a 5-in.-diam lens, and brought to the film so that it overlaps the object beam.

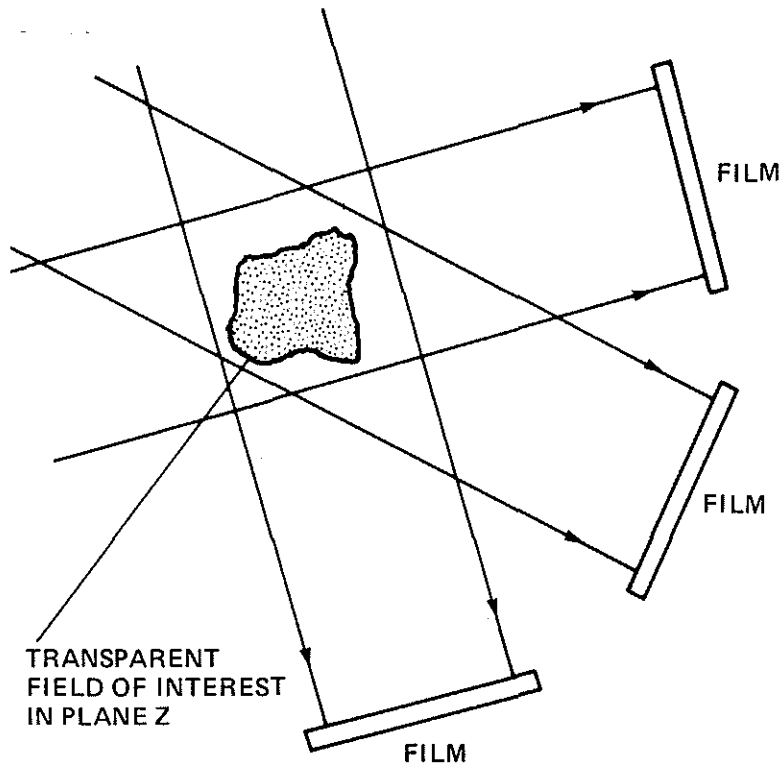


Fig. 7. Recording interferograms at various angles around the field of interest for tomographic reconstruction.

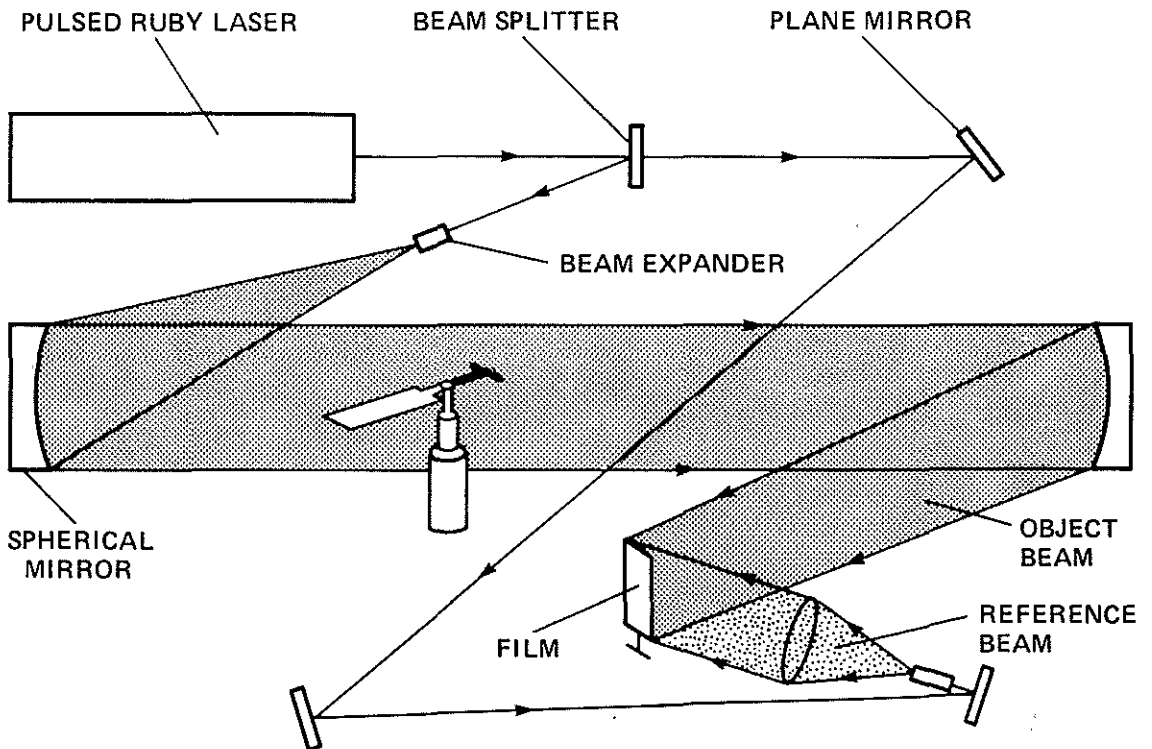


Fig. 8. Schematic drawing of the holographic recording system.

Once the optical system has been aligned, the entire procedure can be controlled from outside the hover chamber. The laser can be fired, the photographic film plates can be changed, and the test conditions can be monitored by remote control. Recall that to record an interferogram, two exposures made at different times (different flow states) must be made on a single film plate. The first exposure is recorded while the rotor blade is stationary, when the air has no velocity and thus has a uniform index of refraction distribution, n_0 . The second exposure is recorded while the blade is rotating at the desired speed. The nonhomogeneous index of refraction distribution in this case introduces phase changes in the second object wave, giving rise to the interference fringes on the film plate. Interferograms were recorded at various angles around the flow by synchronizing the laser pulse with the desired blade position. The photographic plates are then removed from the recording system in the hover chamber, developed, and reconstructed in a laboratory for further processing.

Holographic interferograms were recorded of the flow near a hovering 1/7 geometrically scaled model UH-1H rotor with untwisted NACA 0012 airfoil sections. The blade was run at a tip Mach number of 0.90 such that the flow was transonic and a shock wave was present in the flow.² Two blades are normally run on the Aeromechanics test stand; however, in views near chordwise, the optical beam passes through an index of refraction field on each blade. The index of refraction field from one blade cannot be separated from the other; therefore, a single-bladed rotor with a counter balance is used. Interferograms at 40 different angles of view were recorded.

4. RESULTING HOLOGRAPHIC INTERFEROGRAMS

The first holographic interferograms of the flow near a transonic rotor blade have been recorded and several are presented in this section. Figure 9 is a simplified schematic plan view of the optical system near the blade area. The blade rotates in a clockwise direction and can be captured at any desired angle of view with the pulsed laser. (It is obviously easier to rotate the blade about the optical system than to rotate the optical system about the blade.) Information about the flow over a large range of viewing angles is required as input to a tomography code. For this experiment, interferograms were recorded from $\theta = 10^\circ$ to $\theta = 190^\circ$, as defined in Fig. 9.

The sketches in Fig. 10 are helpful in interpreting the interferograms. Four different viewing angles are examined in Figs. 10a-10d. The top sketches show plan views of the blade superimposed with approximate contours of constant index of refraction; the lower sketches show the expected appearance

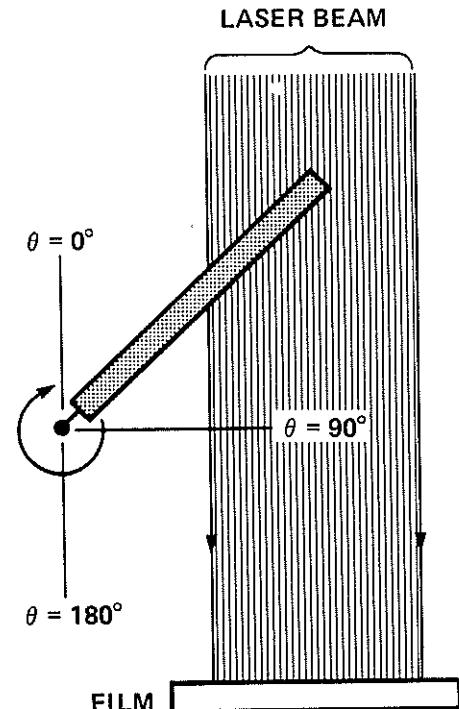


Fig. 9. Angle orientation of rotor blade for recording interferograms (plan view).

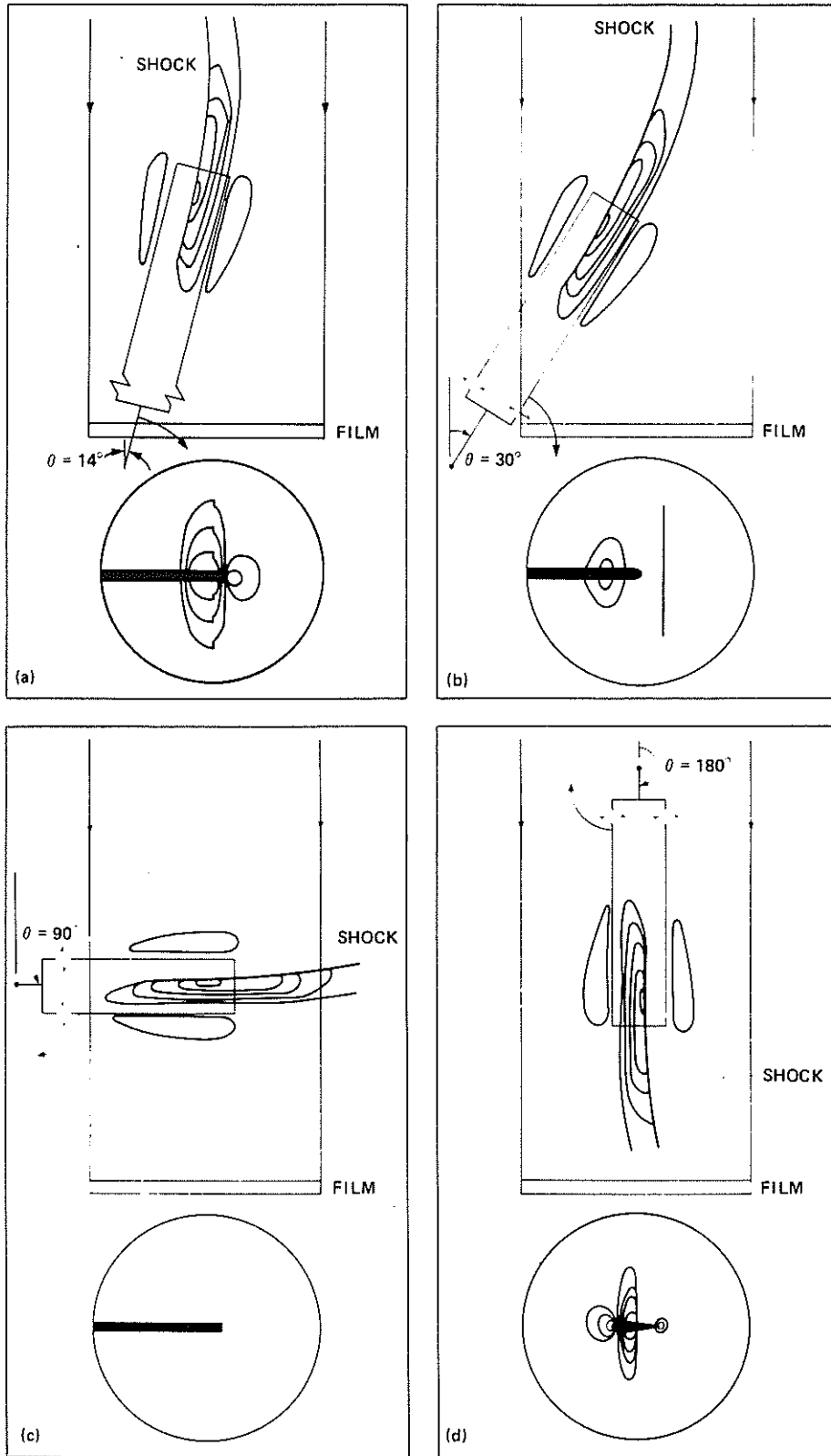


Fig. 10. Plan views of rotor blade with superimposed index of refraction contours, and expected appearance of interferograms at four different viewing angles. (a) $\theta = 14^\circ$. (b) $\theta = 30^\circ$. (c) $\theta = 90^\circ$. (d) $\theta = 180^\circ$.

of the interferograms. Recall that if an optical ray passes through a strong (or "long") index of refraction field its optical path length is changed substantially, which would give rise to many fringes on an interferogram. Conversely, if an optical ray passes through a very weak (or "thin") index of refraction field its optical path length is changed very little, which would give rise to very few interference fringes.

At $\theta = 14^\circ$ (Fig. 10a), the optical rays pass through a very long portion of the index of refraction field; thus, numerous fringes would appear in the interferogram near the blade tip. The shock wave would be most noticeable where it is parallel to the optical rays, and in this case the shock would appear "inside" the blade tip. At $\theta = 30^\circ$ (Fig. 10b), the optical rays pass through a thinner portion of the same index of refraction field; thus, only a few fringes will appear. Now, the section of the shock wave that is parallel to the optical rays is "outside" the blade tip and would be indicated at this location in the interferogram. At $\theta = 90^\circ$, or the spanwise view (Fig. 10c), very few or no fringes will appear since an optical ray passes through a very thin portion of the index of refraction field. Since no part of the shock wave is parallel to the optical rays, no evidence of a shock wave will be visible in the interferogram. At $\theta = 180^\circ$, or the chordwise view (Fig. 10d), many interference fringes will be present since the optical ray passes through the longest portion of the index of refraction field. Also, the shock wave will be seen on the blade surface in great detail.

Some of the holographic interferograms at various angles around a transonic rotor blade are presented in Figs. 11-20. In many of these figures, the blade tip has been highlighted for clarity, and key features of the flow have been identified. Also, note that the shadow of the rotor system taken in the first exposure (blade stationary) appears in several interferograms. This shadow blocks the information at this location, but does not affect the fringe pattern. At $\theta = 14^\circ$ (Fig. 11), the gradient on the blade surface appears fairly large. The leading-edge stagnation point can be clearly seen and the tangential portion of the shock appears on the blade in the region of the gradient. At $\theta = 24^\circ$ (Fig. 12), the gradient appears only moderately intense on the blade surface. The tangential portion of the shock has "moved" away from the gradient region closer to the blade tip. It appears that the presence of the shock in the vicinity of the blade tip obscures the leading-edge stagnation point in this view. At $\theta = 30^\circ$ (Fig. 13), the gradient on the rotor blade now appears quite small. The tangential portion of the shock is now located beyond the blade tip and the unobscured leading-edge stagnation point can be seen once again. As the blade's azimuthal angle increases, the gradient appearance continues to decrease and the tangential portion of the shock continues to "move" farther from the blade tip. At $\theta = 90^\circ$, or the spanwise view (Fig. 14), no evidence of the gradient on the blade surface can be seen. The shock is not visible, because the optical rays pass through the very thin cross section of the shock. Only a few background (noise) fringes are observed. At $\theta = 166^\circ$ (Fig. 15), the gradient on the blade surface once again appears to increase since the optical rays pass through a longer portion of the index of refraction field. It is difficult to identify the exact location of the shock in this view. Since the shock is still at a moderate angle to the viewing direction, only a "smeared" shock can be observed.

At very large azimuthal angles (Figs. 16-20), the interferograms contain most of the important "two-dimensional-like" features of the transonic flow field near the tip of the rotor. At $\theta = 176^\circ$ (Fig. 16), the

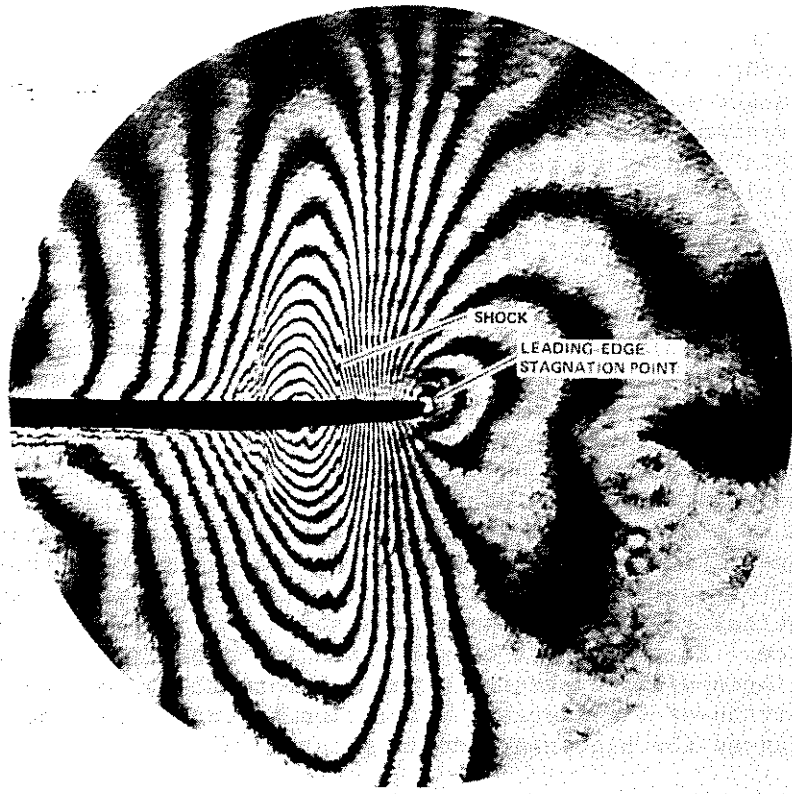


Fig. 11. Interferogram recorded at 14° .

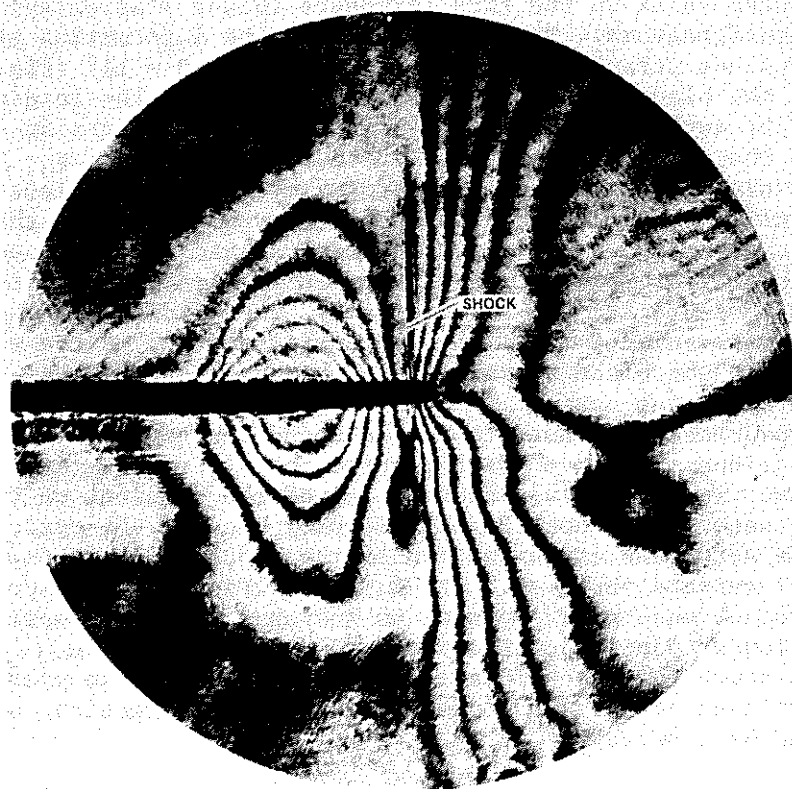


Fig. 12. Interferogram recorded at 24° .

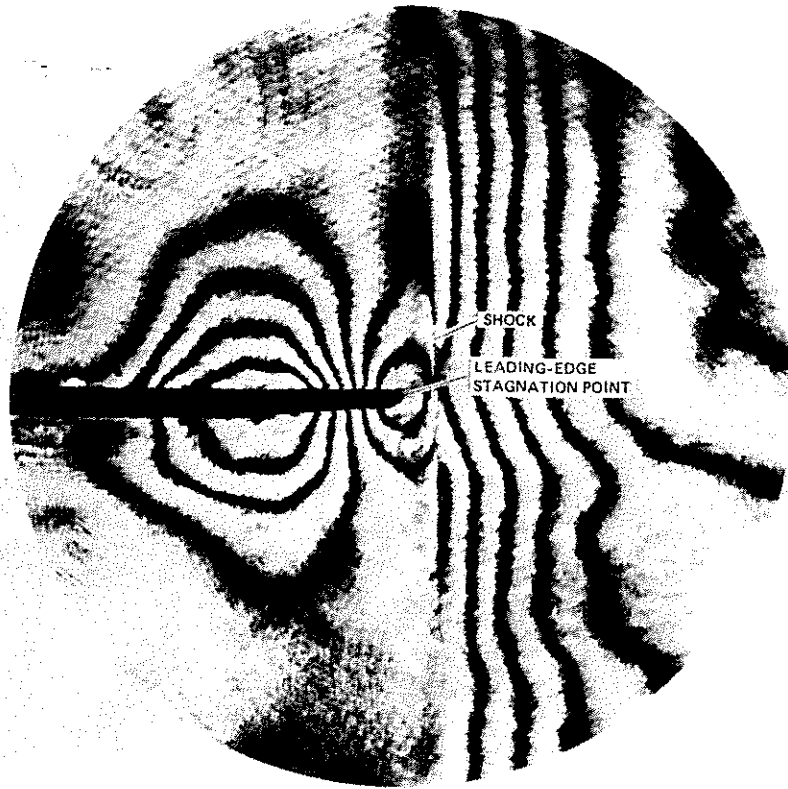


Fig. 13. Interferogram recorded at 30° .



Fig. 14. Interferogram recorded at 90° (spanwise view).

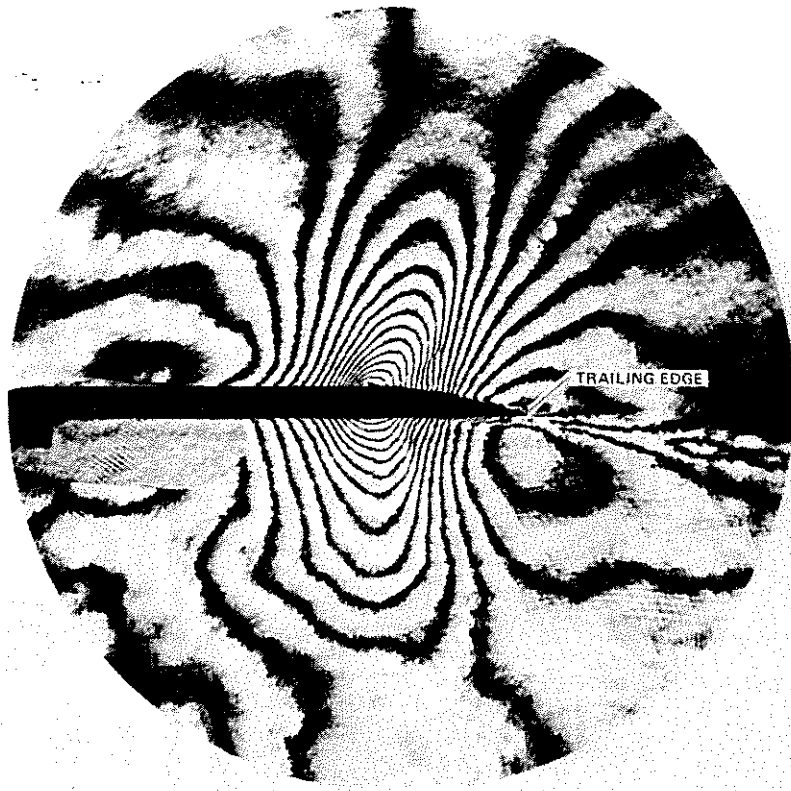


Fig. 15. Interferogram recorded at 166° .

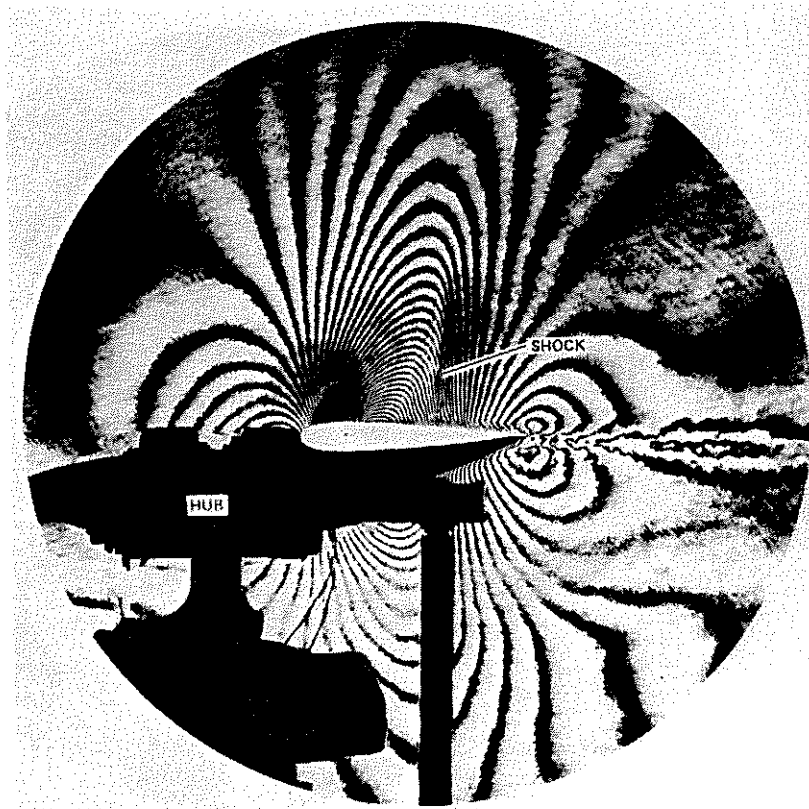


Fig. 16. Interferogram recorded at 176° .

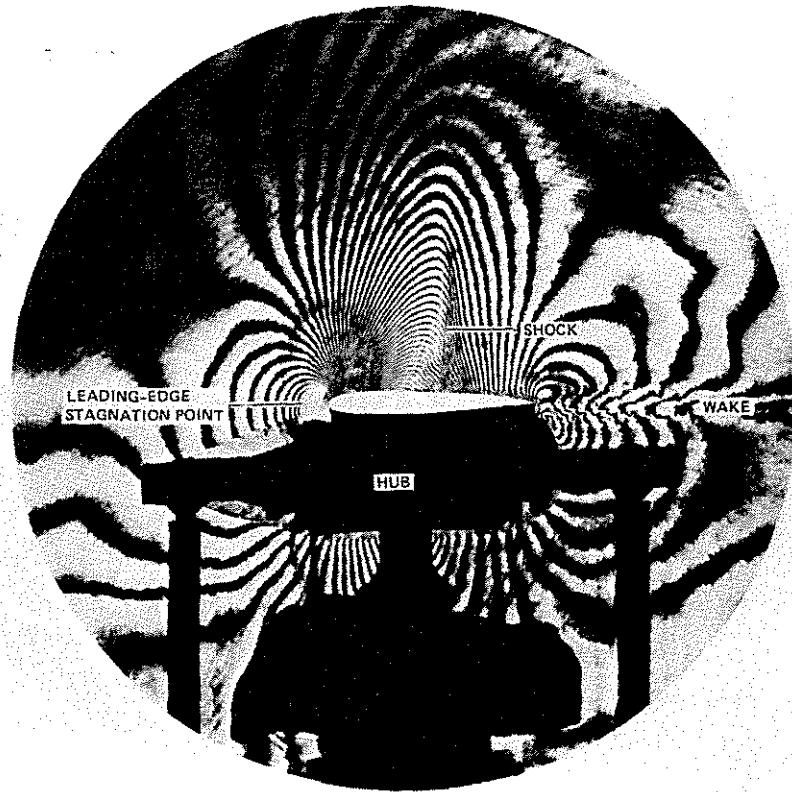


Fig. 17. Interferogram recorded at 180° (chordwise view).

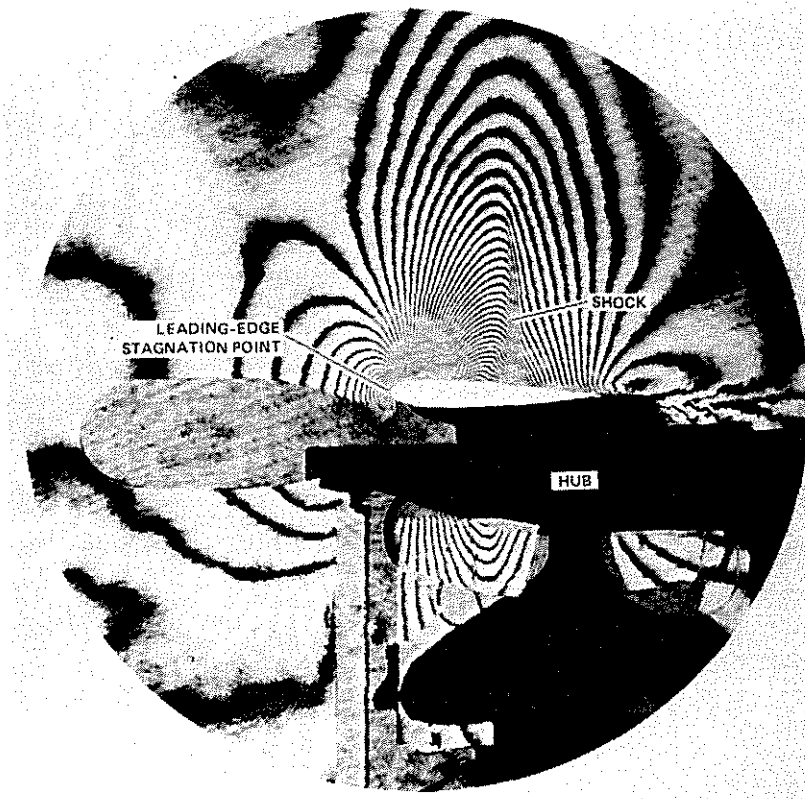


Fig. 18. Interferogram recorded at 182° .

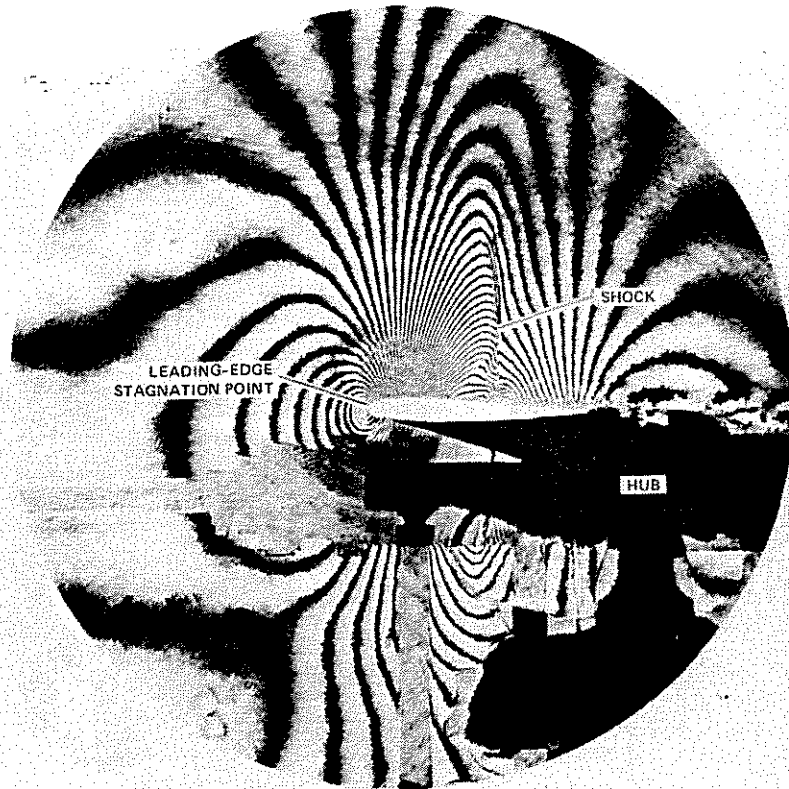


Fig. 19. Interferogram recorded at 184° .

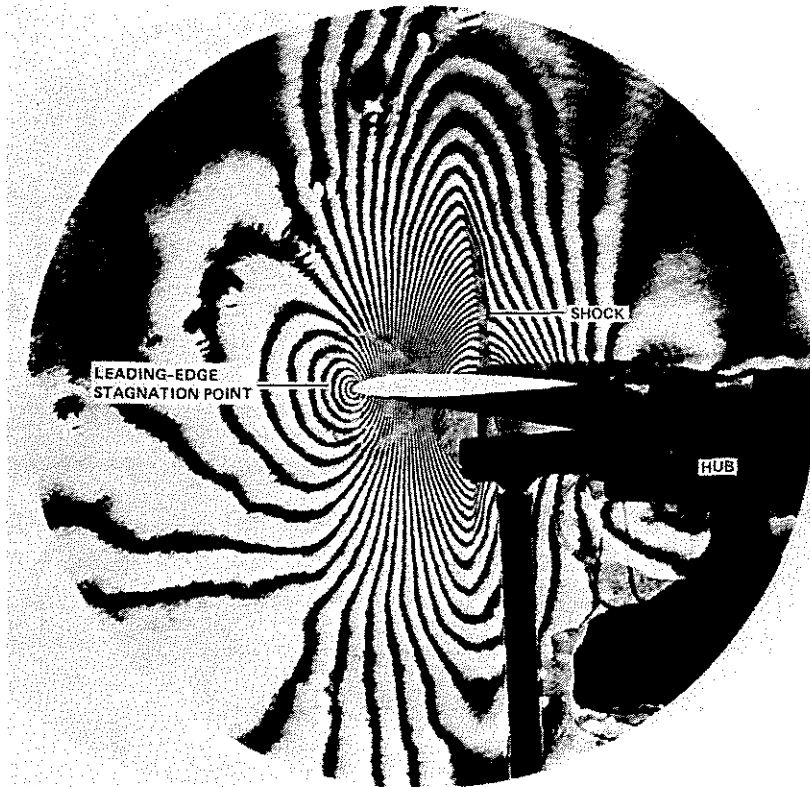


Fig. 20. Interferogram recorded at 186° .

gradient appears very strong on the blade surface. The shock is much less "smeared" and begins to take on the appearance of a lambda shock. Its location on the blade surface can be easily identified. At $\theta = 180^\circ$, or the spanwise view (Fig. 17), the blade is pointing directly out of the page. At this angle, the gradient on the blade surface appears to be at a maximum. The lambda shock is clearly visible, for the shock is nearly tangential to the optical rays. In addition, the small Reynolds number ($\sim 10^6$) of the NACA 0012 airfoil is seen to induce lambda-shock/boundary-layer interactions, which causes the flow to separate. At $\theta = 182^\circ$ (Fig. 18) and at $\theta = 184^\circ$ (Fig. 19), the intensities of the gradient on the blade surface and of the leading-edge stagnation point appear to decrease slightly, as expected. The shock is very distinct, for it is now approximately parallel to the optical rays. At $\theta = 186^\circ$ (Fig. 20), the shock on the blade surface appears to "spread" very slightly since the optical rays pass through the shock region at a slight angle once again.

These last few interferograms (Figs. 16-20) demonstrate the tremendous potential of holographic interferometry for use in investigations of transonic rotor flow fields. The entire "two-dimensional-like" flow field is seen with the clarity that is more typical of steady two-dimensional transonic flows. Exact integrated density variations throughout the entire flow field can be obtained by simply counting fringes. (The details of this procedure are summarized in the Appendix.) For a three-dimensional flow, information must be extracted from several angles of view to yield accurate quantitative results. Fortunately, the high quality of the interferograms at all azimuthal angles makes the tomographic reconstruction process a reality.

5. CONCLUDING REMARKS

Holographic interferometry has proved to be a very effective method for recording interferograms of the flow near a transonic rotor blade. The insensitivity of the technique to optical-equipment quality makes it quite suitable to the rugged environments of rotor testing. Numerous high-quality interferograms have been recorded showing quantitative flow characteristics of a hovering transonic rotor. In the views that are dominated by two-dimensional phenomena, flow details near and off the blade are shown with outstanding quality - including attached and detached shocks, shock-induced flow separation, and regions of high and low density. Data from these interferograms taken at many azimuthal angles can now be supplied to a computer tomography code to compute properties of the three-dimensional flow field at any desired point. This method makes it possible to obtain quantitative, nonintrusive measurements of a large-scale three-dimensional compressible flow field in a relatively short test time.

6. APPENDIX

On an interferogram, quantitative information is represented in the fringe pattern, as given by Eq. (8). To obtain more useful quantities (i.e., density), Eq. (8) can be written as

$$\Delta\Phi = \int_s [\rho(x,y,z) - \rho_0] ds = \frac{N\lambda}{k} \quad (10)$$

where index of refraction is related to density by the Gladstone-Dale equation:

$$N = k\rho + 1$$

where k , the Gladstone-Dale constant, is a property of the gas. To solve Eq. (10), the fringe order-number N must be obtained from the interferogram. This means assigning numbers to the fringes. Under ideal conditions assigning fringe numbers is straightforward; however, a few comments should be made in this regard. First, the fringe $N = 0$ must be determined; it corresponds to a region in the flow where the field is "undisturbed." Second, it must be determined whether the fringes should be assigned positive or negative values. A positive value may correspond to an increase in density, and a negative value may correspond to a decrease in density. To assign the correct fringe order numbers, some previous knowledge of the flow is helpful. In the case of the transonic flow near a rotor blade, it is known that the air is relatively undisturbed far from the blade, that a high-density region exists at the stagnation point, and that a low-density region exists on the blade surface. With this prior knowledge, the information can be given to a tomography code in the form of the fringe order number, its coordinate position on the interferogram, and the viewing angle of the interferogram.

REFERENCES

- 1) F. H. Schmitz and Y. H. Yu, "High Speed Rotor Noise and Transonic Aerodynamics," AIAA Paper 80-1009, AIAA 6th Aeroacoustics Conference, Hartford, Conn., June 1980.
- 2) F. H. Schmitz and Y. H. Yu, "Transonic Rotor Noise - Theoretical and Experimental Comparisons," Vertica, 5, 1981, pp. 55-74.
- 3) F. X. Caradonna, "The Transonic Flow on a Helicopter Rotor," Ph.D. dissertation, Stanford U., Stanford, Calif., Mar. 1978.
- 4) J. D. Trolinger, "Laser Instrumentation for Flow Field Diagnostics," AGARDograph 186, 1974.
- 5) D. A. Johnson and W. D. Bachalo, "Transonic Flow about a Two-Dimensional Airfoil - Inviscid and Turbulent Flow Properties," AIAA Paper 78-1117, July 1978.
- 6) W. D. Bachalo, "Measurements of Supercritical Airfoil Flow Fields Using Interferometry," Douglas Aircraft Company, McDonnell Douglas Corporation, Mar. 1982.
- 7) R. D. Matulka and D. J. Collins, "Determination of Three-Dimensional Density Fields from Holographic Interferometry," Journal of Applied Physics, 42, 1971, pp. 1109-1119.
- 8) D. W. Sweeney and C. M. Vest, "Reconstruction of Three-Dimensional Refractive Index Fields from Multidirectional Interferometric Data," Applied Optics, 12, 1973, pp. 2649-2664.
- 9) C. M. Vest, Holographic Interferometry, Wiley-Interscience, 1979.
- 10) R. J. Collier, C. B. Burckhardt, and L. H. Lin, Optical Holography, Academic Press, 1971.



NINTH EUROPEAN ROTORCRAFT FORUM
13-15th Sept. 1983 - STRESA - ITALY

PAPER NUMBER: 1

TITLE: "Measurement of the Instantaneous
Velocities in a Helicopter Rotor Wake
in Forward Flight"

AUTHORS: H. VELKOFF, R. NAVARRO, H. TERKEL
Department of Mechanical Engineering
The Ohio State University
Columbus, Ohio 43210